



# De-coupling the Eigenmodes of SMA-reinforced Bimorph Composites using Multi-objective Optimization

Rupal Srivastava<sup>1</sup> · Bishakh Bhattacharya<sup>2</sup>

Received: 13 July 2021 / Revised: 22 February 2022 / Accepted: 18 March 2022  
© Krishtel eMaging Solutions Private Limited 2022

## Abstract

**Introduction** Autonomous shape and vibration control of a structure expand its utility, thereby increasing the need for adaptive composites in the field of aerodynamics, civil, space, and mechanical engineering. One way to achieve this is by reinforcing composites with smart materials like shape memory alloy (SMA) wires or ribbons, piezoelectric (PZT) materials, and magnetostrictive materials.

**Objectives** In this study, the authors optimize the numerically solved bending behavior of SMA fiber-reinforced E-glass fiber-Silicone matrix composite upon thermal actuation. The study is shown for four cases (a) single layer of SMA embedded unimorph, (b) two-layers of SMA embedded bimorph, (c) single layer SMA embedded bimorph with a honeycomb core, and (d) single layer SMA embedded bimorph with an auxetic core. The vibration responses of these cases upon analysis show that the first three eigenmodes of the unimorph and the bimorph SMA composite include bending and torsion modes and the corresponding eigenfrequencies are significantly close in magnitude for the Austenite finish ( $A_f$ ) temperature. In other words, the first natural frequency displays complex eigenmodes. A multi-objective optimization approach for SMA hybrid composite plates for de-coupling eigenfrequencies is proposed in this study.

**Methods** The Non-dominated Sorting Genetic Algorithm (NSGA-II) is used to minimize the eigenfrequency corresponding to the first bending eigenmode and maximize the eigenfrequency corresponding to the first twisting eigenmode, thus increasing the effective difference between the two eigenfrequencies. The authors also simultaneously maximize the deflection of the structures in order to obtain a considerable morphing observation. The present investigations involve determining the best laminate configuration relying on SMA fiber angle orientation and SMA ply thickness as the variables.

**Results** A complex mode or a combination of two modes at the first eigenfrequency or complex modes can cause failure of the structure, making decoupling an essential requirement. The algorithm proposed can also be used to interchange the eigenmodes of their corresponding eigenfrequencies, thus allowing the first natural frequency to give a twisting or torsional eigenmode and the consecutive natural frequency that of a bending mode. This technique can be used to avoid Phugoid motion-based failure in an aircraft by continuously controlling and interchanging the eigenmodes of its wings.

**Keywords** Shape memory alloys · Adaptive composites · NSGA II · Multiobjective optimization · De-coupled eigenfrequency · Structural optimization

## Introduction

Adaptive composites are becoming increasingly popular due to their superior adaptive characteristics, like variable stiffness, making it amenable to tailoring structural, damping, and vibration responses. Exceptional variations in such composites' mechanical and vibration response can be achieved by altering the lay-up, the volume fraction of fibers, fiber-angle orientation, and ply thickness. Thus, adaptive composites offer the prospect to create an extensive set of various structural output tailored for specific needs. Several smart materials are being used as

✉ Bishakh Bhattacharya  
bishakh@iitk.ac.in

Rupal Srivastava  
rupal.srivastava@tus.ie

<sup>1</sup> Confirm Smart Manufacturing, Science Foundation Ireland, Technological University of the Shannon: MM, Athlone, Ireland

<sup>2</sup> Department of Mechanical Engineering, Indian Institute of Technology, Kanpur, Ireland

reinforcements to fabricate an adaptive composite; some of them are shape memory alloys, piezoelectric materials, and magnetostrictive particulate composites. The idea of embedding SMAs in a laminated polymer matrix composite (PMC) was first given by Rogers and Robertshaw [1], thereafter continuously exploring its application in structural acoustic control [2], and active control of sound radiation from panels [3]. In active property tuning [4], one takes advantage of the increase in elastic modulus caused due to transformation of prestrained SMA wires from their martensite state to the austenite state. Substantial work has been carried out to utilize the properties of SMA embedded composites- improvement of impact damage resistance [5], enhancement of critical buckling loads, and post-buckling response [6]. Bhaskar et al. compile the major applications of SMA embedded composites as short and long fibers [7].

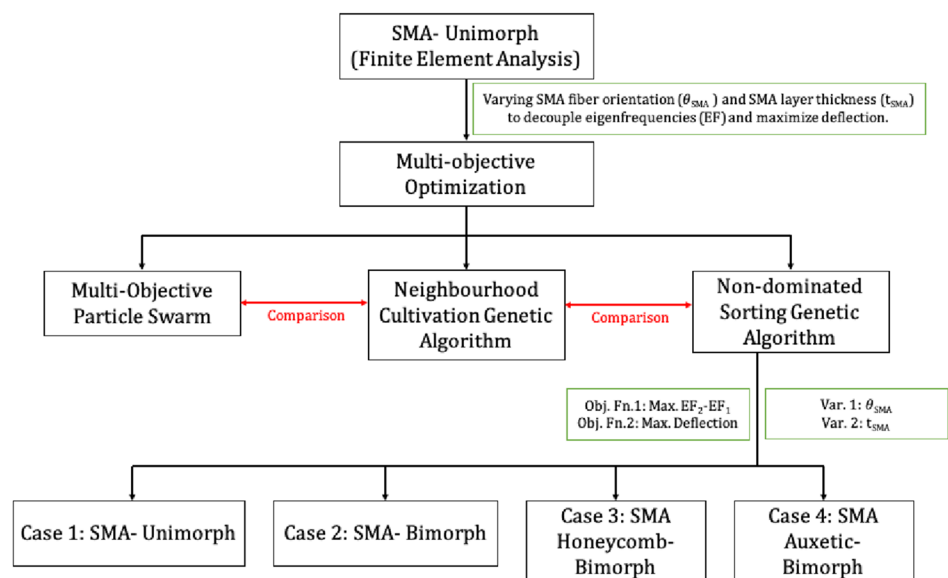
Shape memory alloys have also found application in morphing structures, one such major application being the use of NiTi alloy for active jet engine chevron to reduce jet engine noise during take-off [8]. Another significant application of shape memory alloy hybrid composite (SMAHC) was the optimal design of a variable-twist propeller that changes the built-in twist in an adaptive manner [9]. The shape morphing behavior of the shape memory alloy composites can also be availed in deployable applications, thus widening the scope of SMAHC in the field of origami-based folding [10]. Embedding shape memory alloy wires in thin membranes has also been studied to demonstrate the effect on the aerodynamic profile of an aircraft wing [11]. The shape morphing property of the SMAHCs is also finding extensive use in robotics- a biomimetic jellyfish [12] and a turtle-like swimming robot [13] are some notable examples.

Given the immense engineering opportunities opened up by such composites, it became crucial to optimize the required applications' structures. One of the earliest works in this domain

was done by Schmit and Farshi, where they used the inscribed hyperspheres optimization algorithm to achieve minimum weight optimum design of laminated fiber composite plates, subject to multiple in-plane loading conditions [14]. Using Genetic Algorithm (GA), Riche and Haftkat optimized the laminate stacking sequence for buckling load maximization considering the contiguity and strain constraints [15]. Several optimization problems have been approached for adaptive composites and especially SMA based composites and/or SMA actuation based morphing structures. Haghdoust et al. [16] optimized the shape profile of an SMA sheet in hybrid layered composite structures designed for passive attenuation of flexural vibrations. In another work by Leal et al. [17], a continuous morphing aircraft wing is studied, and the design is optimized to obtain a Pareto frontier to simultaneously minimize cruise airfoil average camber and minimize shape difference between morphed outer mold line and the landing shape. In order to determine the optimal locations in truss structures, optimization techniques such as genetic algorithms (GAs) and simulated annealing (SA) have been used for the corrections of static deformations. Silva et al. [18] used single objective binary-coded GAs and determined optimum voltages needed to apply to the piezoelectric actuators for achieving the desired shape (Fig. 1).

Unlike the most optimization problems solved for SMAHC vibration, to the best of author's knowledge, no literature is found to utilize GA to de-couple eigenfrequencies by optimizing the SMA fiber orientation and SMA ply thickness while minimizing the bending eigenmode and maximizing the twisting eigenmode. The authors implement a methodology that allows them to find a trade-off between the de-coupling of the eigenfrequencies as a desirable output and the complex fabrication of optimized design as an undesirable problem. With this methodology, the authors have an efficiently patterned SMA reinforced composite, which can keep a distinct gap between

**Fig. 1** Flow-diagram of the finite element analysis of the SMA embedded unimorph and bimorph SMAHC, and honeycomb & auxetic ply sample cases, optimization technique comparison and optimization of the sample cases.  $EF_1$ : First eigenfrequency,  $EF_2$ : Second eigenfrequency,  $\theta_{SMA}$ : SMA fiber orientation angle,  $t_{SMA}$ : SMA ply thickness



consecutive eigenfrequencies along with the maximum deflection. The structure has been optimized to perform at the actuation temperature when maximum deflection is obtained upon SMA actuation. The optimization tool is applied to the structure considering a continuous temperature rise, hence an increase in the eigenfrequency of the model, making the present system substantially nonlinear.

The next section discusses the four sample cases' numerical modeling for the thermoelastic and free vibration response analysis. The authors then compare the results of three optimization techniques- Multiobjective Particle Swarm (MOPS), Neighbourhood Cultivation Genetic Algorithm (NCGA), and finally, Non-dominated Sorting Genetic Algorithm (NSGA-II), when applied to the unimorph SMA reinforced composite (Case 1) problem. After the comparative study, the authors validate the model with experimentally obtained results from previous work [19] and extend the NSGA-II technique to three more sample cases.

## Optimization Problem Formulation

In this study, the authors have modelled four SMA embedded Hybrid E-glass fiber-Silicone matrix Composites (SMAHC), (a) a unimorph with single layer of SMA reinforcement, (b) bimorph with two orthogonally placed SMA reinforced layers, (c) bimorph with single layer SMA reinforcement with a honeycomb core, and (d) bimorph with single layer SMA reinforcement with an auxetic core. The Flow-diagram of the finite element analysis of the SMA embedded composites cases is shown in Fig. 1, and the temperature-dependent material properties of the SMA are shown in Fig. 2. The geometric structures of the smart composites considered in the study are shown in Fig. 3. The dimensions of the structures are same for all the four samples along the longitudinal and the transverse directions, however, the thickness varies depending upon the number of layers and inclusion of core.

The input temperature-dependent material properties are limited to the range of room temperature to 66 °C where the maximum dip in the effective coefficient of thermal expansion,  $\alpha$ , is observed. The properties of the E-glass fiber are Young's modulus,  $E_f = 72$  GPa, Poisson's ratio,  $\nu_f = 0.21$ , and coefficient of thermal expansion,  $\alpha_f = 4.9 \times 10^{-6}/^\circ\text{C}$  and the properties of the matrix used as the bonding material are  $E_m = 3.38 \times 10^5$  Pa,  $\nu_m = 0.49$ , and  $\alpha_m = 250 \times 10^{-6}/^\circ\text{C}$  (as provided by the suppliers—E-glass fiber—Azo Materials, Asia, and Silicone rubber-Dragon Skin™ 30, Smooth-On, Pennsylvania, USA).

The finite element model of the composite is created using a 4-node, quadrilateral S4R element that includes the large-strain formulation with reduced integration. The model is defined as a composite in ABAQUS® by defining the equivalent mechanical properties for each layer, including the SMA

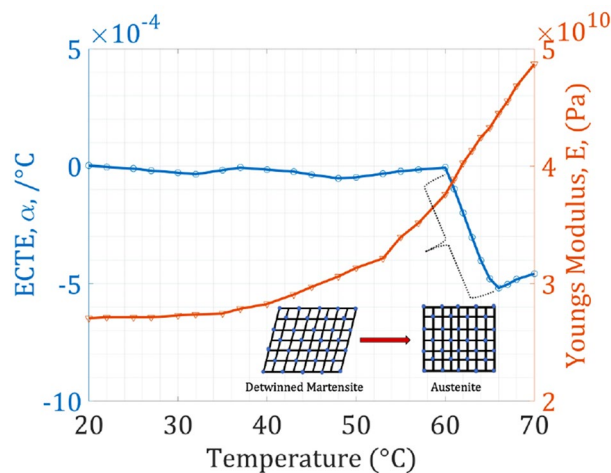


Fig. 2 Experimental data for temperature dependent effective coefficient of thermal expansion and Young's modulus of SMA [20]

layer with temperature-dependent properties. The equivalent properties are calculated using the Lamé's constants and Halpin-Tsai equations [21] as discussed in Appendix 1 and 2. A uniform temperature field is applied to each sample individually, and the corresponding deflection of the composite due to offset embedded SMA's phase-transformation, and hence shape memory effect is recorded. The free-vibration response caused due to linear perturbation is also studied at each temperature step. The authors show a detailed discussion on this analysis in their previous work [19].

The authors next carry out the multiobjective, single variable optimization of Case 1 using three different optimization techniques- Multiobjective Particle Swarm (MOPS), Neighbourhood Cultivation Genetic Algorithm (NCGA), and Non-dominated Sorting Genetic Algorithm-II (NSGA-II) with no constraints at 66 °C where the phase transformation of SMA is completed, and the maximum deflection and frequency are observed. The authors then compare the obtained results and narrow down the technique to one that is then applied to the rest of the sample cases and optimum constraints. In the next section, the comparative study results of the three aforementioned techniques is discussed.

## Comparison Study of the Application of Optimization Techniques

The problem is formulated as per the following optimization function and constraints:

*Objective Functions:*

$$\begin{aligned} \text{Maximize} & : |EF_2(\theta, t) - EF_1(\theta, t)|^2 \\ \text{Maximize} & : U_{\text{mag}}(\theta, t) \end{aligned} \quad (1)$$

*Variables Bound:*

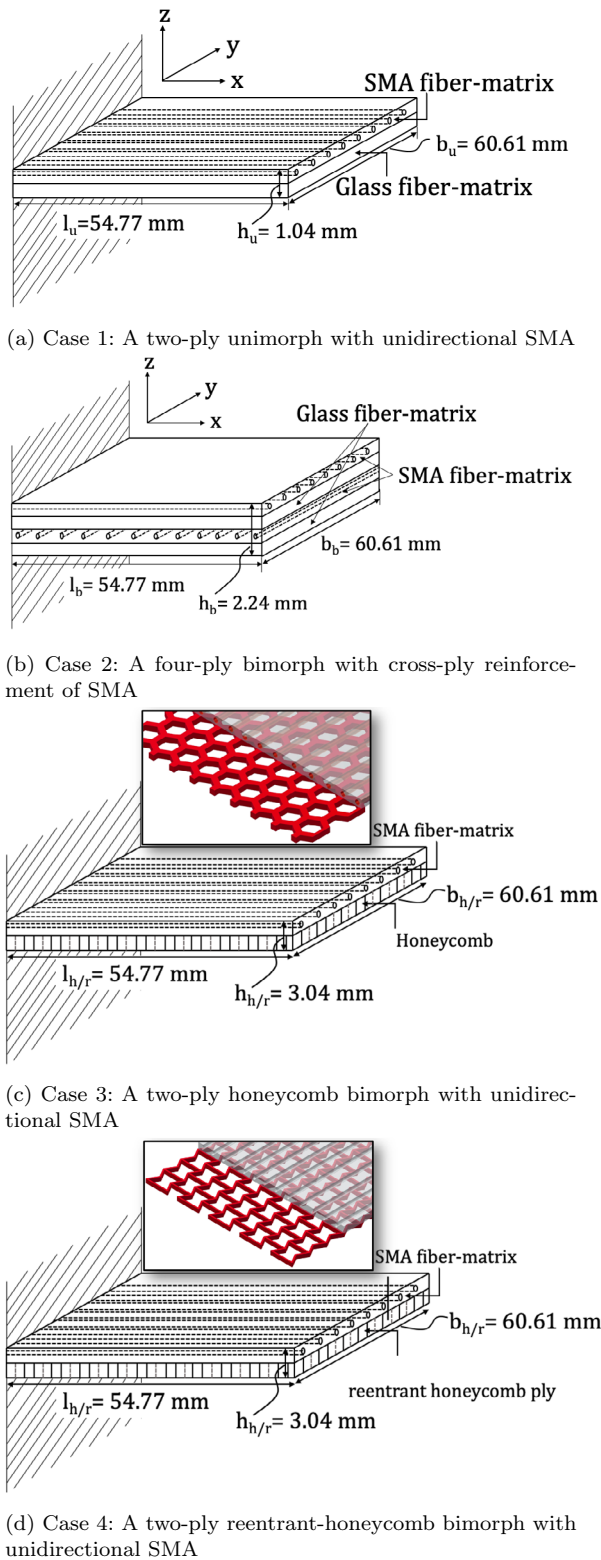


**Fig. 3** Schematic of SMA wire embedded composites- unimorph SMAHC, bimorph SMAHC, and honeycomb/auxetic core SMAHC-laminate configuration and dimensions (non-optimised) [19]

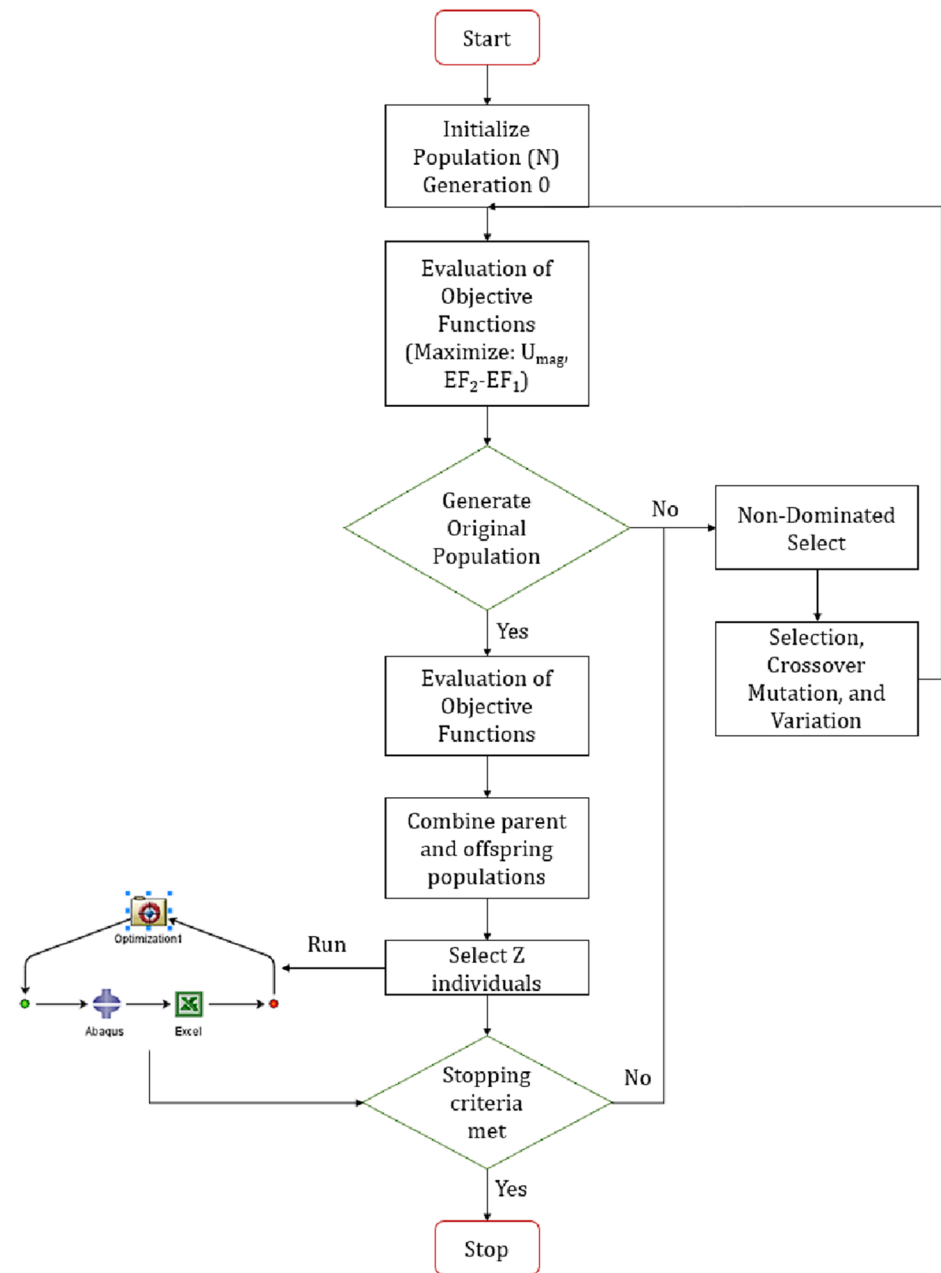
$$\begin{aligned} \text{Variable 1} &: 0^{\circ(L)} \leq \theta_i \leq 90^{\circ(U)} \\ \text{Variable 2} &: 2.5 \times 10^{-4(L)} \leq t_j \leq 1 \times 10^{-3(U)} \end{aligned} \quad (2)$$

where  $EF_1$  is the first eigenfrequency of the composite beam corresponding to the first bending eigenmode,  $EF_2$  is the second eigenfrequency of the composite beam corresponding to the first twisting eigenmode,  $U_{\text{mag}}$  is the maximum displacement of the mid-point along the free edge of the composite,  $\theta$  is the fiber angle orientation,  $t$  is the thickness of the SMA ply lamina, and the indices  $i$  and  $j$  denote the variation of  $\theta$  and  $t$  between the lower and upper bound. In the above optimization problem, the authors have 2–4 design variables depending upon the sample case, three conflicting nonlinear objective functions, and three inequality constraints. out of the three conflicting objectives, the authors merge two of them by maximizing the difference between the minimizing first eigenfrequency and maximizing the second eigenfrequency, hence making this essentially a bi-objective optimizing problem.

For solving the above multiobjective shape control problem, an integrated optimization approach is proposed, in which the MOPS, NCGA, and NSGA-II optimization techniques are linked with the finite element analysis in ABAQUS<sup>®</sup>. The population size and the number of generations are varied until convergence is obtained, and the crossover probability is 0.9. The proposed algorithm evaluates the various combinations of the SMA fiber orientation ( $\theta$ ) and the SMA ply thickness ( $t$ ) to find the optimal combination of these parameters. The aim is to de-couple bending and twisting eigenmodes, which were observed upon numerical analysis by optimizing the thickness of the SMA ply and orientation of the SMA fibers. The authors simultaneously maximize the deflection behavior making the structure functional for both shape morphing and vibration damping. The temperature field is set to be constant where it gives maximum deflection and the next iteration proceeds. ABAQUS<sup>®</sup> and its sister software iSight<sup>®</sup> are coupled together, to form a bridge to transfer numerical analysis data from ABAQUS<sup>®</sup> to iSight<sup>®</sup> and vice-versa. Figure 4 shows the integration of ABAQUS<sup>®</sup> and iSight<sup>®</sup> for the Optimization Process.

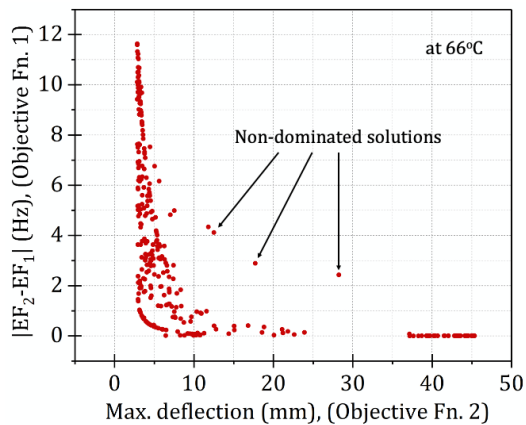
Particle Swarm Optimization (PSO) is a population-based metaheuristic which was originally introduced by [22]. Here *swarm* refers to the population size and a *particle* is an individual member of the *swarm*. For a multiobjective PSO, first, the swarm is initialized, followed by initializing a set of leaders with the nondominated particles from the swarm. Then, a quality measure is calculated for all the leaders in order to select a leader for each particle of the swarm. For every generation, a leader is selected for each particle, and the flight is carried out. After all the particles have been updated, the leaders' set is updated, and their quality measure is re-calculated. When used for the unconstrained Case

**Fig. 4** Flow-diagram of the Abaqus integrated Isight Genetic Algorithm Optimization Process

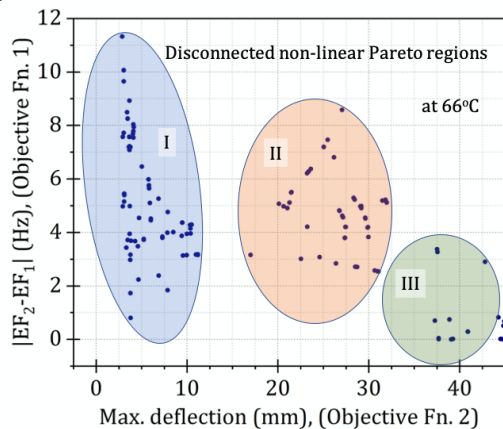


(a) unimorph SMA composite, the authors obtain a conventional Pareto Optimal front. However, it fails to give a maximized solution for both the objective functions, thus leaving the authors to compromise with the deflection in order to decouple the complex eigenmodes. In the Neighborhood Cultivation Genetic Algorithm (NCGA) technique [23], all objective parameters are treated separately, and the standard genetic operation of mutation and crossover is performed. The crossover process is based on the “neighborhood cultivation” mechanism, where the crossover is performed mostly between individuals with values close to one of the objectives. This algorithm, when applied to the unconstrained Case (a), gives a comparatively better solution

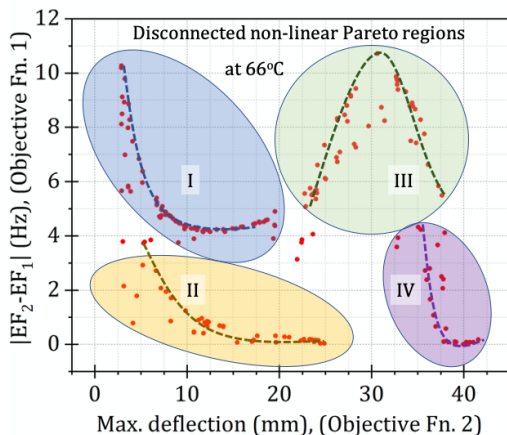
than the previous MOPS method, however the Pareto regions are disconnected and non-linear. Hence, the authors move to the Non-dominated Sorting Genetic Algorithm II [24]. NSGA-II produces offspring’s using a specific type of crossover and mutation. It picks the next generation according to nondominated-sorting and crowding distance comparison. The authors first evaluate the possible combinations without constraining the system, and based on the results, constrain the system and obtain the Pareto-Optimal front. As can be seen in Fig. 5c, a disconnect non-linear Pareto Optimal region is obtained for unconstrained Case (1), however, a benefitting solution region is observed in region III where both the objective functions can be seen maximized. Various



(a) Multi-Objective Particle Swarm- gives an explicit Pareto Optimal front when no constraints are included in the algorithm.



(b) Neighbourhood Cultivation Genetic Algorithm with no constraints- gives disconnected non-linear Pareto regions.



(c) Non-dominated Sorting Genetic Algorithm with no constraints- gives disconnected non-linear Pareto regions. The third region contains the solution as per the requirements.

**Fig. 5** Comparison study of **a** Multi-objective Particle Swarm, **b** Neighbourhood Cultivation Genetic Algorithm, and **c** Non-dominated Sorting Genetic Algorithm applied to the defined optimization problem. Case **(a)** Unimorph SMAHC with no constraints, variables- thickness of SMA ply ( $t_{SMA}$ ) and SMA fiber angle orientation ( $\theta_{SMA}$ )

steps in the NSGA-II optimization algorithm are described below:

1. Setting the NSGA-II parameters such as population size, number of generations, and crossover probability.
2. Initializing the population  $N$ .
3. For each population member, decide the SMA fiber orientation angle and the SMA layer's thickness from the lower and upper bound values of the design variables. For the current study, the finite element model of the SMAHC is created with SMA wires as reinforced fibers.
4. The corresponding finite element analysis is carried out in ABAQUS for each population member to obtain the deflection and natural frequency within the given temperature range.
5. The obtained values are substituted back into the NSGA-II via the Simulink bridge in iSight®.
6. Evaluation of the objective function and the constraints values.
7. Performing nondominated sorting of the population and assigning front-ranking.

The further steps of the algorithm follow the generic steps of the optimization problem, such as creating offspring using selection, crossover, and mutation operators, combining of parent and offspring population, calculating the crowding distance, and replacing the old parent population with the new child population. Finally, the authors repeat the same steps for the next generation until the defined number of generations is reached. The results of the three techniques with the same set of variables and objective functions are shown in Fig. 5. As can be seen, MOPS gives a convex Pareto Optimal Set, and the NCGA and NSGA-II give disconnected Pareto Optimal sets. However, to maximize both the objective functions, the authors need a technique that can give a non-convex Pareto Optimal set. The desired set of solutions was found in Region- III of the NSGA-II Pareto solutions; the authors then constrain the problem accordingly to achieve the non-convex set of solutions discussed in the next section.

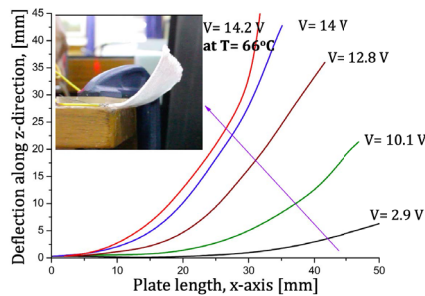
## Results and Discussion

### Case 1: SMA Unimorph

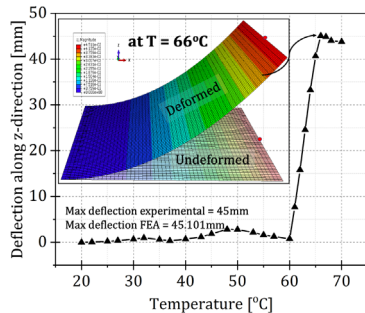
In this case, the authors consider the SMAHC with a single layer of SMA reinforcement. Since the SMA is embedded at an offset (refer Fig. 3a), upon thermal actuation the phase transformation in the SMA causes it to contract to its parent austenite state, and the entire structure gives bending along the  $z$ -direction. It can intuitively be

observed that the maximum deflection will be obtained in this case when the SMA fibers are oriented along with the longitudinal direction of the composite. The authors first get the Pareto-optimal solutions for the single objective optimization problem by varying the SMA fiber orientation angle with  $0^\circ$  and  $90^\circ$  as lower and upper bound, respectively. The finite element solution for this case with  $0^\circ$  SMA fiber orientation produces a maximum deflection in the structure of 45.101 mm. The authors validate the result with their experimental observations from their previous work [19], wherein a unimorph SMA-reinforced composite is fabricated with the given dimensions and material properties. An average of 45mm deflection was observed in the structure upon complete phase transformation of the SMA, as shown in Fig. 6.

The authors also give a linear perturbation to the structure to analyze its dynamic response. Here, the authors observe numerically that both the first and the second natural frequencies are 41.79Hz, and the corresponding eigenmodes are symmetric-out-of-plane bending and twisting, respectively [19]. This makes the system chaotic as it is observed that two modes at the same frequency are resulting in a complex mode. Hence, the authors de-couple the frequencies by minimizing the first and maximizing the second natural frequency. The results corresponding to the de-coupling of



(a) SMAHC unimorph deflection- Experimental observation [Srivastava et al. (2018)]. The deflection corresponding to voltage,  $V=14.2$  V at  $T=66^\circ\text{C}$  is considered for numerical observation shown in Figure 6b.

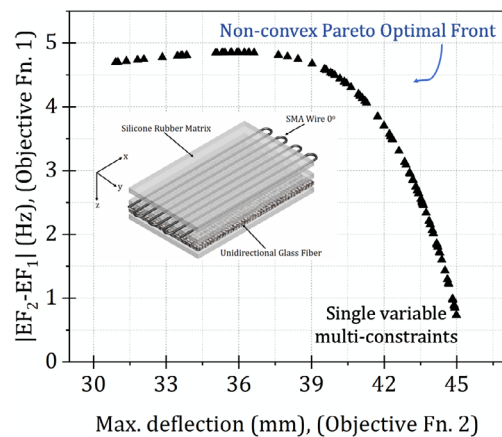


(b) SMAHC unimorph deflection- Numerical observation. The inset image shows the simulated deflection at  $T=66^\circ\text{C}$ .

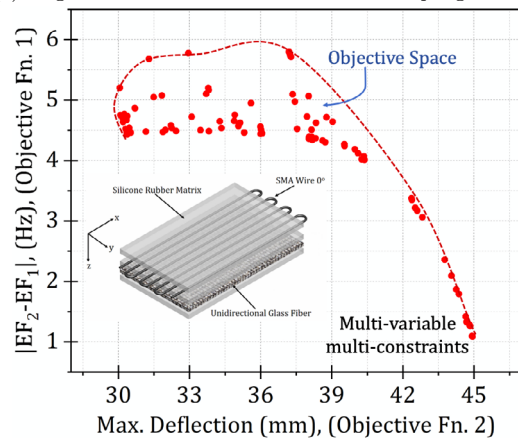
**Fig. 6** Validation of the numerical model against experimental results [19], SMA fiber volume fraction,  $(V_f^{\text{SMA}})=0.024$ , E-glass fiber volume fraction,  $(V_f^{\text{EGF}})=0.7$ , SMA fiber orientation angle,  $(\theta^{\text{SMA}})=0^\circ$

frequencies and maximizing the deflection are shown in Fig. 7a. It is further observed that by a considerable change in the  $\theta$  the authors were able to extract a twist from the structure; however, by slightly changing the orientation angle to  $1.43^\circ$  from  $0^\circ$ , the authors get almost 5Hz of frequency de-coupling with a 17.5% reduction in bending performance to 37.20 mm from 45.101 mm (refer to Table 1).

The authors then carried out the same set of steps with both SMA orientation angle and SMA layer thickness as variables and constraining the system to get a minimum of 30 mm of deflection. In this case, the authors get a set of Pareto-optimal solutions and an objective space, as shown in Fig. 7b. Here, the authors are able to increase the deflection by approximately 2 mm by keeping the orientation angle the same as obtained in the single-variable case and reducing the thickness by 0.03 mm. A larger objective space allows to choose the input variables for even more sophisticated and accurate results. The non-convex Pareto-optimal Solution that is obtained does not give linear relation of the variation in  $\theta_{\text{SMA}}$  and  $t_{\text{SMA}}$ . The multiobjective optimization



(a) Single variable-  $\theta$  with deflection and decoupling bounds.



(b) Multi-variable-  $\theta$  and  $t$ , with deflection and decoupling bounds.

**Fig. 7** Pareto Optimal Curve for the unimorph SMAHC sample case (Case 1)

problem, as stated in Sect. 2 is solved using the proposed iSight-ABAQUS integrated optimization algorithm. The total computation time for solving this on a computer with an Intel Core™ i7 processor is estimated at around 20 h.

### Case 2: SMA Bimorph

In the second case (refer to Fig. 3b) the maximum deflection obtained from the structure when analyzed numerically is 0.5mm in the opposite direction. This reduction in bending is caused due to orthogonal placement of SMA fibers causing a bending constraint to each other. However, by changing the SMA fiber orientation angles for both the plies, the authors experience a twist in the structure with subsequent de-coupling of the modes. Hence, the de-coupling of the modes, in this case, was obtained at the expense of considerable twisting in the structure. The high amount of twist gives a large deflection along the  $z$ -direction; the applications of this sample case with the given ply lay-up are confined to domains where twisting of the structure is either required or has to be neglected, as can be seen in Fig. 8.

### Case 3: SMA Bimorph with Honeycomb Core

In this case, the SMA fibers are placed along the longitudinal direction of a honeycomb core. The honeycomb core gives the structure a saddle-shaped deflection caused due to the contraction in the SMA upon temperature increase. This bimorph deflection behavior can be utilized where the active shape morphing requires an overall negative Gaussian curvature. As shown in Fig. 9, similar to the previous cases, a significant difference in the SMA fiber orientation angle

from  $0^\circ$  can cause a significant twist in the system. Hence, to maintain a bimorph bending without noticeable twisting with the de-couple natural frequency, the authors select the Pareto-optimal solution with the least  $\theta$  variation. The saddle-shape is a limiting case of the inner surface of the Torus structure. Shape control of such skewed-composites is useful in applications like controlling the shape of airfoil and torus-like structures (Fig. 9).

### Case 4: SMA Bimorph with Auxetic Core

Lastly, the authors apply the NSGA-II optimization to the SMA reinforced bimorph with the reentrant-honeycomb (auxetic) core. The SMA fibers are placed along the longitudinal direction of the auxetic core and thermally actuated. The maximum deflection and the first and second eigenfrequencies are recorded after the SMA phase transformation. The optimizing technique is applied at this temperature to maximize the deflection and the second eigenfrequency and minimize the first eigenfrequency, thus de-coupling the two frequencies. Similar to previous cases, as the authors maximize the de-coupling, a twisting in the structure is experienced; however, keeping the  $\theta$  variation between  $0^\circ$  and  $90^\circ$  keeps the twisting minimal with considerable de-coupling. Figure 10 gives the Pareto Optimal set of solutions for this case where a large amount of de-coupling can be seen as the structure experiences twisting. Table 1 shows the shift in the deformation and eigenfrequency data with a slight change of  $\theta$  from  $0^\circ$  to  $0.85^\circ$ .

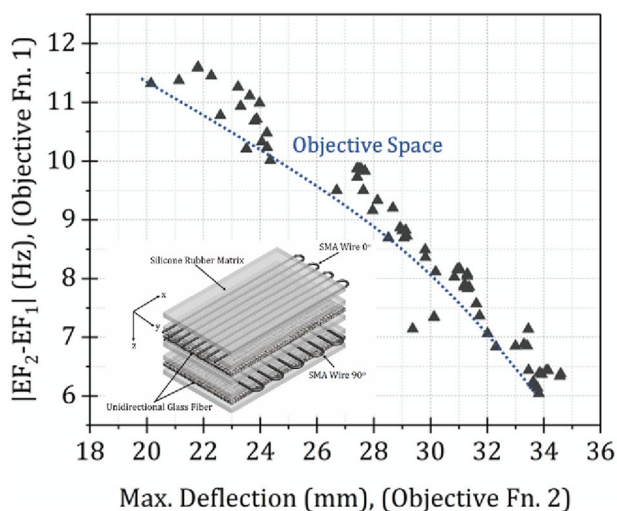


**Fig. 8** Pareto Optimal Curve for the bimorph SMAHC sample case (Case 2), multi-variable- $\theta$  and  $t$ , with deflection and decoupling bounds

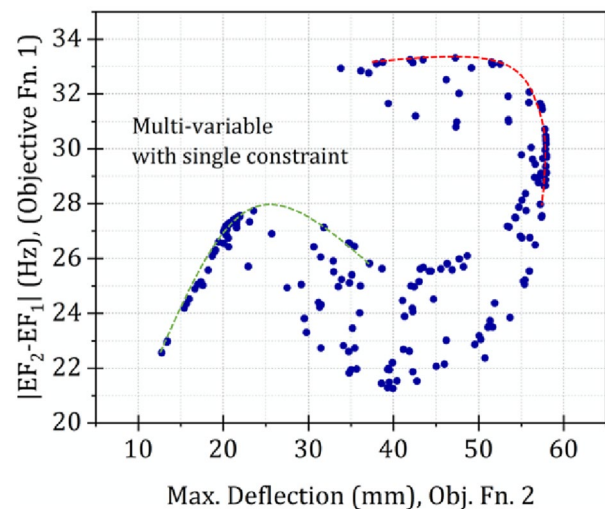


**Fig. 9** Pareto Optimal Curve for the bimorph SMAHC with honeycomb ply sample case (Case 3), multi-variable- $\theta$  and  $t$ , with only deflection bounds

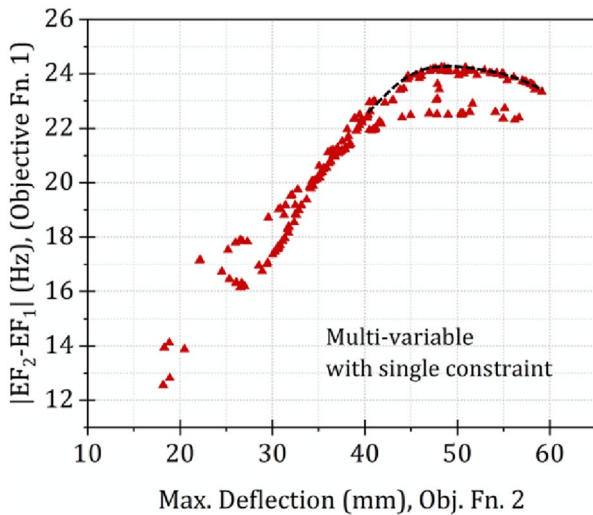


**Fig. 10** Pareto Optimal Curve for the bimorph SMAHC with reentrant-honeycomb ply sample case (Case 4), multi-variable- $\theta$  and  $t$ , with only deflection bounds

**Table 1** Optimized vs non-Optimized deflection and eigenfrequencies for the four sample cases

Case no.	$\frac{\text{normalize Non-Optimized}}{\text{normalize Optimized}}$	Deflection (along z-direction) mm	First Eigenmode (bending) Hz	Second Eigenmode (twisting) Hz
1	$\theta = 0^\circ$ $t = 0.54$ mm	45.10	41.79	41.79
	$\theta = 1.43^\circ$ $t = 0.61$ mm	37.20	38.02	43.82
2	$\theta_1 = 0^\circ$ $\theta_2 = 90^\circ$ $t_1 = 0.54$ mm $t_2 = 0.54$ mm	-0.49	38.47	38.49
	$\theta_1 = 10.8^\circ$ $\theta_2 = 40.4^\circ$ $t_1 = 0.97$ mm $t_2 = 0.97$ mm	27.7	36.10	45.93
3	$\theta = 0^\circ$ $t = 0.54$ mm	19.73	24.73	75.38
	$\theta = 0.18^\circ$ $t = 0.5$ mm	20.36	24.54	51.74
4	$\theta = 0^\circ$ $t = 0.54$ mm	20.11	26.67	40.29
	$\theta = 0.85^\circ$ $t = 0.63$ mm	19.68	26.53	39.71

**Conclusions**

In this paper, the authors have presented a comparative study of MOPS, NCGA, and NSGA-II optimization

techniques for a multi-variable SMA reinforced composite showing unimorph bending upon SMA thermal actuation. Subsequently, three optimization studies corresponding to the maximization of compliance and fundamental natural frequencies in bending and torsion are carried out. This is further treated as multiple objective problems to maximize the deflection of the unimorph while separating the band gap between bending and twisting mode. The active shape control problem is formulated as a multiobjective optimization problem. An algorithm has been proposed based on a population eigenmodes used to evaluate the variable bounds of the objective functions. The authors validated the convergence of the obtained Pareto Optimal solution by comparing it with single-objective solutions. The finite element model is also successfully validated with the experimental response values. The authors envisage the studies will provide interesting design input for the smart flap development related to UAVs and UMVs in the near future. This work will be further continued for the optimization of honeycomb and reentrant honeycomb strut dimensions and reentrant angles and their cumulative effect on the deflection and contribution to the eigenmode decoupling. The authors will also determine the weight of each variable contributing to the optimized solution using Shapely Values method, and consider the twisting of the structure during the bimorph bending to further reduce or enhance the twisting based on the application and requirement of the problem.

**Appendix 1: A Turner’s Effective Coefficient of Thermal Expansion Model (ECTE)**

Turner’s ECTE model gives constitutive equations for predicting the thermomechanical response of SMA hybrid composite structures subjected to combined thermal and mechanical loads [25]. The model is valid for restrained, free recovery, as well as constrained behavior of SMA, given that the authors possess data for basic SMA material properties. The ECTE model captures the material nonlinearity of the SMA with respect to temperature and the mechanics of composites with embedded SMA actuators. A representative volume element employed in Turner’s model is shown in Fig. 11. This element is considered in the plane of the plate, the principal material directions are 1 and 2, wherein the SMA wire is embedded along 1-direction.

For a SMAHC lamina of Glass-Epoxy embedded with NiTiNOL wires, adding the thermal expansion behavior of NiTiNOL from Turner, Zhong, and Mei [26] to the 1D uniaxial thermoelastic constitutive relation by Jia and Rogers [27]:

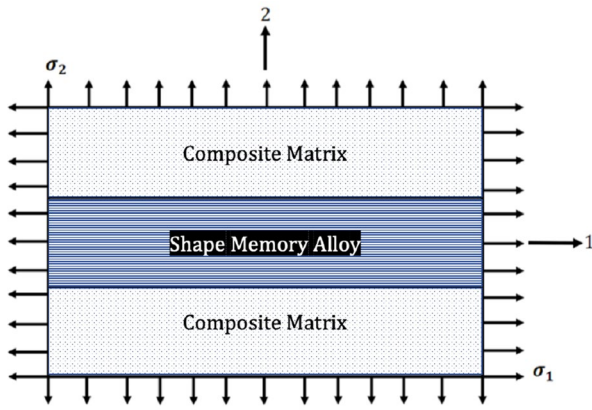


Fig. 11 Volume element of the SMAHC lamina [25]

$$\sigma_{1a} = E_a \epsilon_1 + \sigma_r \quad T \geq A_s \tag{3a}$$

$$\sigma_{1a} = E_a (\epsilon_1 - \alpha_{1a} \Delta T) \quad T < A_s \tag{3b}$$

Here,  $E_a$  is the Young’s Modulus of the SMA,  $\epsilon_1$  is the strain in 1-direction (longitudinal),  $\alpha_{1a}$  is the coefficient of thermal expansion for SMA when temperature  $T$  is less than the austenite start temperature  $A_s$ , and  $\sigma_r$  is the recovery stress of the SMA when  $T \geq A_s$ .

The uniaxial thermoelastic constitutive relation for SMA written in terms of Effective Coefficient of Thermal Expansion (ECTE) is:

$$\sigma_{1a} = E_a \left[ \epsilon_1 - \int_{T_0}^T \alpha_{1a}(\tau) d\tau \right] \tag{4}$$

From Eqs. (3a), (3b) and (4) we see that at temperature below Austenite start temperature,

$$\int_{T_0}^T \alpha_{1a}(\tau) d\tau = \alpha_{1a} \Delta T \tag{5}$$

and at temperatures above austenite start temperature,

$$\begin{aligned} \sigma_r &= -E_a \int_{T_0}^T \alpha_{1a}(\tau) d\tau \\ \text{or, } \int_{T_0}^T \alpha_{1a}(\tau) d\tau &= -\frac{\sigma_r}{E_a} \end{aligned} \tag{6}$$

Using the above equations we can capture the non-linear thermoelastic behavior of the SMA. Similarly, the constitutive equation for the transverse direction is:

$$\sigma_{2a} = E_a \left[ \epsilon_2 - \int_{T_0}^T \alpha_{2a}(\tau) d\tau \right] \tag{7}$$

In the case of SMA wires reinforced unidirectionally along 1-direction  $\alpha_{2a}$  is not related to recovery stress but is linear due to change in martensite fraction. Thus, the thermoelastic constitutive relations for an orthotropic lamina under plane stress becomes:

$$\begin{pmatrix} \sigma_1 \\ \sigma_2 \\ \tau_{12} \end{pmatrix} = \begin{bmatrix} Q_{11} & Q_{12} & 0 \\ Q_{12} & Q_{22} & 0 \\ 0 & 0 & Q_{66} \end{bmatrix} \begin{pmatrix} \epsilon_1 \\ \epsilon_2 \\ \gamma_{12} \end{pmatrix} - \begin{bmatrix} Q_{11} & Q_{12} & 0 \\ Q_{12} & Q_{22} & 0 \\ 0 & 0 & Q_{66} \end{bmatrix} \int_{T_0}^T \begin{pmatrix} \alpha_1 \\ \alpha_2 \\ 0 \end{pmatrix} d\tau \tag{8}$$

where  $[Q]$  is the reduced stiffness matrix; the above constitutive relation is referred to as the effective coefficient of thermal expansion model (ECTEM). The relation between the reduced stiffness matrix and the engineering constants, Rule-of-Mixtures, and Halpin-Tsai equations are discussed in B.

The authors employed ECTEM in their work due to the following main reasons:

1. The authors do not require the superelastic effect for constrained recovery analysis; this model suitably predicts the required Shape Memory Effect.
2. The model requires only four parameters- Austenite Start Temperature, Austenite Finish Temperature, Recovery Stress, and Young’s Modulus, and the authors had resources available to calculate the same.

### Appendix 2: Reduced Stiffness Matrix and Rule-of-Mixtures

$$Q_{11} = \frac{E_1}{1 - \nu_{12}\nu_{21}} \quad Q_{12} = \frac{\nu_{12}E_2}{1 - \nu_{12}\nu_{21}} \tag{9}$$

$$Q_{22} = \frac{E_2}{1 - \nu_{12}\nu_{21}} \quad Q_{66} = G_{12}$$

$$\begin{aligned} E_1 &= E_a V_a + E_m V_m & E_2 &= \frac{E_a E_m}{E_a V_m + E_m V_a} \\ \nu_{12} &= \nu_a V_a + \nu_m V_m & G_{12} &= \frac{G_a G_m}{G_a V_m + G_m V_a} \\ \int_{T_0}^T \alpha_1(\tau) d\tau &= \frac{E_a V_a \int_{T_0}^T \alpha_a(\tau) d\tau + E_m V_m \int_{T_0}^T \alpha_m(\tau) d\tau}{E_a V_a + E_m V_m} & \text{sgn}(\alpha_a) &= \begin{cases} +1 & T < A_s \\ -1 & T \geq A_s \end{cases} \end{aligned} \tag{10}$$

$$\int_{T_0}^T \alpha_2(\tau) d\tau = \int_{T_0}^T [\alpha_a(\tau) V_a + \alpha_m(\tau) V_m] d\tau$$

where the subscripts  $a$  and  $m$  indicate SMA/fiber and matrix constituents, respectively,  $E, \nu, G, \alpha$  are the Young’s modulus, Poisson’s ratio, shear modulus, and effective coefficient

of thermal expansion respectively,  $V_a$  and  $V_m$  are the SMA/ fiber and matrix volume fraction respectively.

**Acknowledgements** The authors are thankful to Dr. Rituparna Datta for invaluable suggestions in the initial stages of the article and Dr. Arun K. Sharma for his contribution in reviewing the manuscript. R.S. would also like to acknowledge project IUSSTF/ME/2017400A for partial funding of this work.

## References

- Rogers CA (1988) Novel design concepts utilizing shape memory alloy reinforced composites. In: Proceedings of the American Society of Composites 3rd Technical Conference on Composite Materials (Technomic), pp 719–731
- Rogers CA, Liang C, Fuller CR (1990) Modeling of shape memory alloy hybrid composites for structural acoustic control. *J Acoust Soc Am* 89:1. <https://doi.org/10.1121/1.400503>
- Rogers CA, Fuller CR, Liang C (1990) Active control of sound radiation from panels using embedded shape memory alloy fibers. *J Sound Vib* 136:1. [https://doi.org/10.1016/0022-460X\(90\)90947-X](https://doi.org/10.1016/0022-460X(90)90947-X)
- Srivastava R, Kumar R, Bhattacharya B (2020) Vibration response studies of a bi-morph sma hybrid composite using 3d laser doppler vibrometer. In: Proceedings of the ASME 2020 Conference on Smart Materials, Adaptive Structures and Intelligent Systems <https://doi.org/10.1115/SMASIS2020-2231>
- Paine JSN, Rogers CA (1994) High velocity impact response of composites with surface bonded nitinol-SMA hybrid layers. *J Intell Mater Syst Struct* 5:4. <https://doi.org/10.2514/6.1995-1409>
- Ro J, Baz A (1995) Nitinol-reinforced plates: Part II static and buckling characteristics. *Compos Eng* 5:77–90. [https://doi.org/10.1016/0961-9526\(95\)93981-Z](https://doi.org/10.1016/0961-9526(95)93981-Z)
- Bhaskar J, Sharma A, Bhattacharya B, Adhikari S (2020) A review on shape memory alloy reinforced polymer composite materials and structures. *Smart Mater Struct* 29(7):073001. <https://doi.org/10.1088/1361-665x/ab8836>
- Hartl D, Lagoudas D, Mabe J, Calkins F (2009) Use of ni60ti shape memory alloy for active jet engine chevron application, part I: thermomechanical characterization. *Smart Mater Struct* 19:1. <https://doi.org/10.1088/0964-1726/19/1/015020>
- Park JS, Kim SH, Jung SN (2011) Optimal design of a variable-twist prop rotor incorporating shape memory alloy hybrid composites. *Compos Struct* 93:2288–2298. <https://doi.org/10.1016/j.compstruct.2011.03.017>
- Peraza Hernandez E, Hartl DJ, Galvan E, Malak R (2013) Design and optimization of a shape memory alloy-based self-folding sheet. *J Mech Des* 135:11. <https://doi.org/10.1115/1.4025382>
- Simpson JC, Boller C (2008) Design and performance of a shape memory alloy-reinforced composite aerodynamic profile. *Smart Mater Struct* 17:025028. <https://doi.org/10.1088/0964-1726/17/2/025028>
- Villanueva A, Smith C, Priya S (2011) A biomimetic robotic jellyfish (robjelly) actuated by shape memory alloy composite actuators. *Bioinspir Biomim* 6:036004. <https://doi.org/10.1088/1748-3182/6/3/036004>
- Kim HJ, Song SH, Ahn SH (2013) A turtle-like swimming robot using a smart soft composite (SSC) structure. *Smart Mater Struct* 22:014007. <https://doi.org/10.1088/0964-1726/22/1/014007>
- Schmit A, Farshi B (1973) Optimum laminate design for strength and stiffness. *Int J Numer Methods Eng* 7:519–536. <https://doi.org/10.1002/nme.1620070410>
- Riche RL, Haftkat RT (1993) Optimization of laminate stacking sequence for buckling load maximization by genetic algorithm. *AIAA J* 31:951–956. <https://doi.org/10.2514/3.11710>
- Haghdoust P, Cinquemani S, Conte AL, Lecis N (2017) Optimal design of damping layers in SMA/GFRP laminated hybrid composites. *Smart Mater Struct* 26(10501):5–13. <https://doi.org/10.1088/1361-665X/aa87dc>
- Leal PB, Petterson R, Hartl DJ (2017) Design optimization toward a shape memory alloy-based bio-inspired morphing wing. In: AIAA/AHS Adaptive Structures Conference 25. <https://doi.org/10.2514/6.2017-0054>
- Silva S, Ribeiro R, Rodrigues J, Vaz M, Monteiro J (2004) The application of genetic algorithms for shape control with piezoelectric patches- an experimental comparison. *Smart Mater Struct* 13:220–226. <https://doi.org/10.1088/0964-1726/13/1/026>
- Srivastava R, Bhattacharya B (2020) Thermoelastic and vibration response analysis of shape memory alloy reinforced active bimorph composites. *Smart Mater Struct* 30:015033. <https://doi.org/10.1088/1361-665x/abc56d>
- Srivastava R, Sharma AK, Hait AK, Bhattacharya B (2018) Design and development of active bimorph structure for deployable space application. In: Proc. SPIE 10595, Active and Passive Smart Structures and Integrated Systems XII, 105953E, <https://doi.org/10.1117/12.2296547>
- Halpin JC (1969) Stiffness and expansion estimates for oriented short fiber composites. *J Compos Mater* 3:732–734. <https://doi.org/10.1177/002199836900300419>
- Kennedy J, Eberhart R (1995) Particle swarm optimization. In: Proceedings of ICNN'95 - International Conference on Neural Networks, Perth, WA, Australia, vol.4, pp 1942–1948, <https://doi.org/10.1109/ICNN.1995.488968>
- Deb K (2001) Multi-objective optimization using evolutionary algorithms. Wiley, New York
- Deb K, Pratap A, Agarwal S, Meyarivan T (2002) A fast and elitist multiobjective genetic algorithm: NSGA-II. *IEEE Trans Evol Comput* 6(2):182–197. <https://doi.org/10.1109/4235.996017>
- Turner TL, Zhong W, Mei C (1994) Finite element analysis of the random response suppression of composite panels at elevated temperatures using shape memory alloy fibers. *AIAA J*. <https://doi.org/10.2514/6.1994-1324>
- Turner T, Zhong Z, Mei C (1994a) Finite element analysis of the random response suppression of composite panels at elevated temperatures using shape memory alloy fibers. In: 35th Structures, Structural Dynamics and Materials Conference 1324
- Jia J, Rogers CA (1994) Formulation of a mechanical model for composites with embedded SMA actuators. In Proceedings of the 35th structures. Structural Dynamics and Materials Conference. <https://doi.org/10.2514/6.1994-1324>

**Publisher's Note** Springer Nature remains neutral with regard to jurisdictional claims in published maps and institutional affiliations.